Advanced Powder Technology 32 (2021) 4141–4148

Contents lists available at ScienceDirect

Advanced Powder Technology

journal homepage: www.elsevier.com/locate/apt

Original Research Paper

Modeling of particle sizes for industrial HPGR products by a unique explainable AI tool- A "Conscious Lab" development

S. Chehreh Chelgani [a,*], H. Nasiri [b,*], A. Tohry [c,d]

[a] Minerals and Metallurgical Engineering, Dept. of Civil, Environmental and Natural Resources Engineering, Luleå University of Technology, SE-971 87 Luleå, Sweden
[b] Department of Computer Engineering, Amirkabir University of Technology, Tehran, Iran
[c] Mining and Metallurgical Engineering Department, Yazd University, Yazd, Iran
[d] Research and Development Unit, Rahbar Farayand Arya Company (RFACo), Tehran, Iran

ARTICLE INFO

Article history:
Received 8 June 2021
Received in revised form 20 August 2021
Accepted 8 September 2021
Available online 20 September 2021

Keywords:
Working gap
Roller speed
Particle properties
Machine learning
XGBoost

ABSTRACT

High-Pressure Grinding Rolls (HPGR), as a modified type of roll crushers, could intensively reduce the energy consumptions in the mineral processing comminution units. However, several problems counted for their operational modeling, especially in the industrial scales. Expanding a conscious laboratory (*CL*) as a recently developed concept based on the recorded datasets from the HPGR operational variables could be tackled those complications and fill the gap. Moreover, constructing such a *CL* base on explainable artificial intelligence (EAI) systems would be an innovative point for the digitalizing powder technology industries. Using a robust EAI model as a strategic approach could significantly improve system transparency and trustworthiness to convert any complicated black-box machine learning to a logical human basis system. This study introduced the SHapley Additive exPlanations (SHAP) and extreme gradient boosting (XGBoost) as the latest powerful EAI tool for the *CL* modeling of the particle sizes produced by an industrial HPGR (P_{80}) in the Fakoor Sanat iron ore processing plant (Kerman, Iran). SHAP precisely assessed multivariable relationships between the monitored operational variables and correlated them with the HPGR P_{80}. SHAP values showed relationship magnitudes among variables and ranked them based on their effectiveness on the P_{80} prediction. The working gap demonstrated the highest importance for the P_{80} prediction. XGBoost could precisely predict the P80 and showed higher accuracy than typical machine learning methods (random forest and support vector regression) for constructing the *CL* of HPGR. These significant outcomes would open a new window for robust consideration of the EAI models within powder technology.

1. Introduction

Around 5% of the generated global electricity consumes annually in mineral processing plants. From this remarkable energy consumption, approximately 80% would be spent in the comminution units (crushing and grinding) [1]. Since the 1980s, the High-Pressure Grinding Rolls (HPGR) as a modified type of roll crushers has been introduced to the ore beneficiation plants to relatively reduce this massive energy ingestion (by around 10–40%) [2,3]. HPGR has been considered a replacement for tertiary crushers and different mills (SAG, ball, and rod mills) [4–7]. Using an HPGR, besides improving energy efficiency, has several advantages for an ore processing plant: high availability, high capacity, and generating micro-cracks in the particles [8,9].

Modeling an HPGR operation and mechanisms involve through its performance would be essential to optimize its production based on the processing plant's desires. The discrete Element Method (DEM) has been recently used for HPGR modeling [10–12]. Barrios and Tavares (2016), using DEM modeling of an HPGR, demonstrated a reasonable agreement between DEM modeling results and phenomenological power models [13]. It was reported that the discharge mass flow rate approximately is independent of axial position, and just a small variation in the confining cheek plate locations would be required to allow weighty axial bypass [14]. DEM also was used to explore the effect of the roll stud diameter on the HPGR capacity and was indicated that it less effect on HPGR throughout and power during grinding [15].

* Corresponding authors.
E-mail addresses: saeed.chelgani@ltu.se (S. Chehreh Chelgani), h.nasiri@aut.ac.ir (H. Nasiri).

https://doi.org/10.1016/j.apt.2021.09.020
0921-8831/

Meanwhile, several mathematical and statistical models have been established to improve the HPGR performance. The generated models mainly focused on the simulation and prediction of power consumption, throughput, and product size distribution [7,16–23]. These models demonstrated high potential, even though they are limited for broad industrial application. Their poor prediction could be mostly addressed as inadequacies of original models and unavailability of all their model input variables in the industrial scales (few operational variables could be measured in the mineral processing plants) [24]. Moreover, assessing these models might require several pilot-scale runs (pilot HPGR tests could accurately scale up to industrial size). However, pilot-scale experiments need a huge quantity of material (1–5 tons) and would be quite costly for new plants [25]. Thus, conscious lab (*CL*), as a most recent development in this area, could be the most accurate solution for tackling all these drawbacks [26,27].

CL as a new concept has been recently developed. A well-structured *CL* assesses and models relationships between operational parameters and their representative responses by using explainable artificial intelligence (EAI) systems and based on the datasets recorded in the industrials scale [26,27]. These models would be a sustainable approach that can directly be used for immediate decision-making in the plants based on the process realities (not optimum theoretical concepts). Using a *CL* could decrease laboratory costs, save time, remove scaling up factors, improve process efficiency and plant maintenance [26,27]. Several different types of machine learning (ML) and AI models have been used for prediction and modeling industrial variables in powder technology. However, these artificial models mostly employed linear or nonlinear regression as the alternate methods and did not present any insight about correlations between monitored operational variables and their representative industrial responses. Therefore, they could be classified as a black box system (not as an EAI model). A comprehensive EAI model as a new digital global framework should be able to assess the correlation between each recorded variable with their representative output, illustrate their correlation magnitude, measure their effectiveness (importance), and rank them based on their importance [28–30].

SHAP (SHapley Additive exPlanations) as a revolutionary through EAI modeling could provide all these assessments for different ML models and improve transparency and trustworthiness [31]. Based on the cooperative (classic) game-theoretic approach, SHAP can explain the output of any AI model and links the optimal credit allocation with local explanations. In other words, Shapley values indicate how each point of a variable can contribute to the prediction, a unique simultaneous linear and nonlinear multivariable assessment [32–35]. SHAP could be coupled with an extreme gradient boosting (XGBoost) model to develop a robust *CL* system for different constructive data assessments. XGBoost as a predictive model followed the Gradient Boosting concept; however, it has several advantages over typical ML models. XGBoost can control over-fitting, handle missing values, and have a dynamic objective function that leads to better performance for the prediction [36–40]. As a novel approach within powder technology, this investigation is going to introduce a *CL* for the prediction of HPGR particle size production (output K_{80}) based on a dataset from the Fakoor Sanat iron ore processing plant by using the SHAP-XGBoost model. Various models (Pearson correlation, random forest, and support vector regression as typical statistical and prediction tools were also considered through the dataset for comparing and assessing the SHAP-XGBoost capability.

2. Materials and methods

2.1. Dataset

For exploring the relationships between HPGR operating variables and their representative P_{80} (output K_{80}), a dataset with 354 records based on monitoring data collected from the Fakoor Sanat iron ore processing plant (Kerman, Iran) from 2018 to 2019 was prepared. In the plant, the HPGR is feeding by low-grade iron ores from dry-stacked tailings. Its capacity is around 235 t/h, and its rolls have 650 mm width and 1100 mm diameter (Fig. 1).

The HPGR products would be feed to a ball mill (Table 1). HPGR key process-operating parameters, including hopper level, roll speed, working gap, hydraulic pressure, fixed and floated power, are monitored by automatic systems and recorded in the main control station of the plant. The feed rate is monitored from deployed belt scale under the belt conveyor. The provided F_{80} (input K_{80}) and P_{80} for the input and output of HPGR streams are the mean value of different recorded F_{80} and P_{80} during each shift. They were determined by sampling and dry sieving analysis in the laboratory. The ratio was determined after measuring the Fe total, and FeO content of the representative samples from HPGR feed by the potassium dichromate titration method (wet chemistry). All these recorded variables were considered for the relationship and modeling assessments.

2.2. Shapley additive exPlanations

The SHapley Additive exPlanations (SHAP) is a game theory-based framework that provides a unified approach to interpreting a machine learning model's predictions and assigns feature importance to input variables [33,41,42]. SHAP is an additive feature attribution method introduced in 2017 by Lundberg and Lee [30]. This method defines the output of a model as a linear addition of input variables. More formally, the SHAP explanation model $g(z')$ for prediction ($f(x)$) is created by decomposing the prediction into a linear function of binary variables $\mathbf{z}' \in \{0,1\}^M$ and SHAP values $\phi_i \in \mathbb{R}$ [43] as expressed in Eq. (1).

$$f(\mathbf{x}) = g(\mathbf{z}') = \phi_0 + \sum_{i=1}^{M} \phi_i z'_i \quad (1)$$

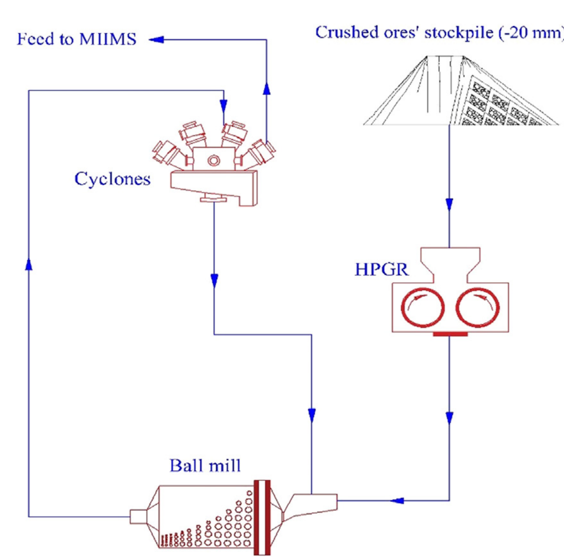

Fig. 1. Simplified comminution units at Fakoor Sanat iron ore processing plant (Kerman, Iran).

Table 1
The statistical description of the HPGR operating variables from the Fakoor Sanat iron ore processing plant.

Variables	Minimum	Maximum	Mean	STD
Feed Rate (t/h)	111	253	188.44	28.67
Hopper Level (%)	47	74	64.53	3.80
Roller Speed (rpm)	413	945	652.00	120.91
Working Gap (mm)	14	29	22.00	2.81
Working Pressure (mm)	165	174	171.03	1.97
Power-FIX (kW)	72	173	116.50	19.08
Power-FLOAT (kW)	48	165	107.45	24.10
Fe (%)	34.98	54.35	46.99	3.15
FeO (%)	2.73	12.60	5.93	1.35
Ratio ($\frac{Fe}{FeO}$) (%)	3.92	18.33	8.36	2.14
F_{80} (mm) (input-K_{80})	5.88	25.51	19.46	3.12
P_{80} (mm) (output-K_{80})	5.04	14.77	9.51	1.69

where M denotes the number of input variables, $\mathbf{z}'$ represents simplified input, and ϕ_0 is the constant value in the absence of all features. SHAP values represent the influence direction of each feature on the model's output [32,35], and can be obtained as the possible solution of Eq. (1) that satisfies three properties: local accuracy, missingness, and consistency. These values can be computed as follows:

$$\phi_i(f,\mathbf{x}) = \sum_{\mathbf{z}' \subseteq \mathbf{x}'} \frac{|\mathbf{z}'|!(M - |\mathbf{z}'| - 1)!}{M!}[f_{\mathbf{x}}(\mathbf{z}') - f_{\mathbf{x}}(\mathbf{z}'^{\smile})] \tag{2}$$

where $\mathbf{x}'$ is the vector of the M selected input variables, f is the trained model, $[f_{\mathbf{x}}(\mathbf{z}') - f_{\mathbf{x}}(\mathbf{z}'^{\smile})]$ specifies the contribution of i th variable in model's output, and $|\mathbf{z}'|$denotes the number of non-zero entries in $\mathbf{z}'$ [41,43].

2.3. Extreme Gradient boosting

Extreme Gradient Boosting (XGBoost) is an efficient and scalable tree boosting algorithm, proposed by Chen and Guestrin in 2016 [44]. Indeed XGBoost is an enhanced version of Gradient Boosted Decision Trees (GBDT), which has proven its capability for pushing the computational power limits for boosted trees [45,46]. XGBoost varies from GBDT in some ways. First, the GBDT method simply employs the first-order Taylor expansion, whereas the loss function used by XGBoost employs second-order Taylor expansion. Additionally, in XGBoost, the objective function is normalized to reduce model's complexity and avoid overfitting [47,48]. Formally, the XGBoost model's predicted output $\hat{y}_i$ is the sum of all scores predicted by K trees, as expressed in Eq. (3).

$$\hat{y}_i = \sum_{k=1}^{K} f_k(\mathbf{x}_i),\ \ f_k \in \Gamma \tag{3}$$

where $\mathbf{x}_i$ is the input feature vector, f_k denotes prediction scores of kth tree (also known as leaf scores), K is the number of regression trees and Γ is the function space containing all possible regression trees [49–51]. To learn the set of functions used in the model, XGBoost tries to minimize the regularized objective function, which is defined in Eq. (4).

$$\phi = \sum_{i=1}^{n} l(y_i, \hat{y}_i) + \sum_{j=1}^{k} \Omega(f_j) \tag{4}$$

where $l(\hat{y}_i, y_i)$ measures the difference between the target y_i and the prediction $\hat{y}_i$, $\Omega(f)$ is the regularization term, which penalizes the complexity of the model to avoid overfitting, and is calculated by Eq. (5).

$$\Omega(f) = \gamma T + \frac{1}{2}\lambda \|\ \omega\ \| \tag{5}$$

where T, ω are the number of leaf nodes and the score on each leaf, respectively.γ, λ are constant coefficients, γ is the complexity cost, and λ is a hyper-parameter for regularization used to adjust regularization degree [51,52].

2.4. Random forest

Random Forest (RF) is a nonparametric supervised machine learning algorithm, which employs ensemble learning techniques for classification and regression [53,54]. The RF presented by Breiman [55] is a combination of Bootstrap aggregating (Bagging) [56] and random variable selection at each node [57]. In other words, it is an extension of bagging that picks a subset of features in each data sample randomly.

The advantages of modeling by the RF include having only a few tunable parameters, resistance to overfitting, having no statistical assumption, and being scale invariant [58–61]. In this study, the random forest regression is used, which builds an ensemble of K trees $\{T_1(\mathbf{x}), T_2(\mathbf{x}), ..., T_K(\mathbf{x})\}$, where $\mathbf{x} = \{x_1, x_2, ..., x_n\}$ is an n-dimensional input vector. Each of these trees generates an estimate $\hat{T}_k(\mathbf{x})$. Then the predictions of the trees are aggregated to form the forest estimate [62–64]:

$$\hat{T}(\mathbf{x}) = \frac{1}{K}\sum_{k=1}^{K} \hat{T}_k(\mathbf{x}) \tag{6}$$

Since each tree $\hat{T}_k(\mathbf{x})$ has low bias and high variance, averaging trees' predictions will stabilize predictions [62,65].

2.5. Support vector regression

The Support Vector Regression (SVR) is a regression method proposed by Drucker based on Vapnik's support vectors concept [66]. The SVR has been shown to be an effective method in estimating real-value functions. One of the key advantages of this method is its computational complexity independent of the input space's dimensionality. In addition, it has a high prediction accuracy and good generalization [67,68].

The SVR can be trained to estimate the regression problem's output and given a training dataset of l samples $T = \{(\mathbf{x}_1, y_1), (\mathbf{x}_2, y_2), ..., (\mathbf{x}_l, y_l)\}$,$\mathbf{x}_i \in \mathbb{R}^n$, $y_i \in \mathbb{R}$. SVR can map observations into a higher dimensional feature space using nonlinear transformation to make them linearly separable. Then there is a linear function (SVR function) in high dimensional space that can formulate non-linear relation between $\mathbf{x}_i$ and y_i as:

$$f(\mathbf{x}) = \mathbf{w}\phi(\mathbf{x}) + \mathbf{b} \tag{7}$$

where $f(\mathbf{x})$ represents the estimated values of the mapped points, $\phi(\mathbf{x})$ is a feature mapping function, $\mathbf{w}$ and $\mathbf{b}$ are the weight and bias,

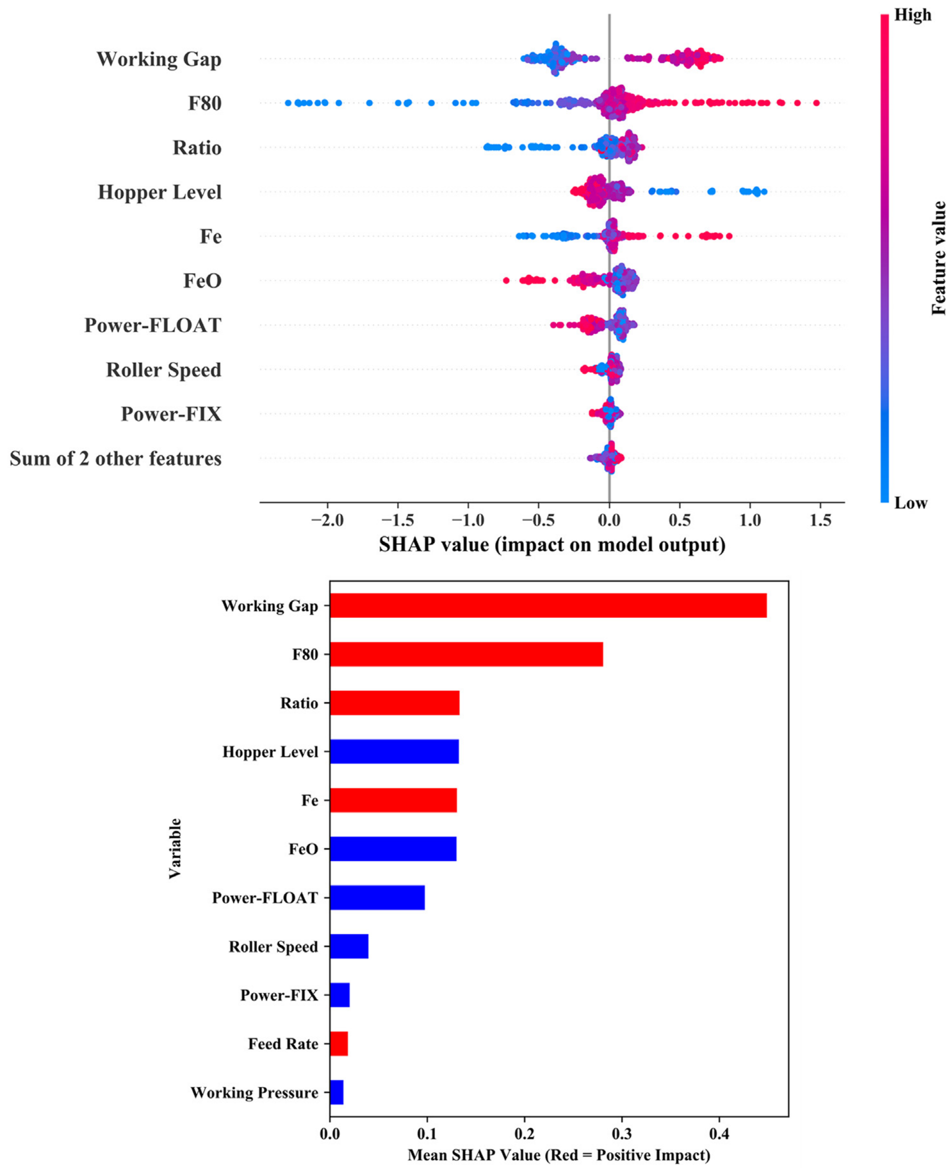

Fig. 2. SHAP analysis of variables for the P_{80} (K_{80}-output) prediction.

respectively [69,70]. **w** and **b** are determined by minimizing the objective function (Eq. (8)) subject to constraints (Eq. (9)).

$$\min_{\mathbf{w}} R(\xi_i, \xi_i^*, \mathbf{w}) = \frac{1}{2}\| \mathbf{w} \| + C\sum_i(\xi_i + \xi_i^*) \tag{8}$$

$$\text{s.t.}\begin{cases} y_i - \mathbf{w}\phi(\mathbf{x}_i) - \mathbf{b} \leqslant \varepsilon + \xi_i \\ -y_i + \mathbf{w}\phi(\mathbf{x}_i) + \mathbf{b} \leqslant \varepsilon + \xi_i^* \\ \xi_i \geqslant 0; \quad \xi_i^* \geqslant 0 \end{cases} \tag{9}$$

where ε is the permitted error threshold, $\{\xi_i\}_{i=1}^{l}, \{\xi_i^*\}_{i=1}^{l}$ are slack variables, and the constant C is the regularization parameter. The value of ε determines the radius of the tube (ε-tube) around the approximated function. The SVR does not penalize data points that fall inside this tube since they are considered as correct predictions. ξ, ξ^* are employed to compute the distance between the target values and ε-tube's boundary values. C is used to balance model complexity and the empirical risk [70–72]. After solving Eq. (8), the $f(\mathbf{x})$ can be obtained as follows:

$$f(\mathbf{x}) = \sum_i(\alpha_i^* - \alpha_i)K(\mathbf{x}_i, \mathbf{x}) + \mathbf{b} \tag{10}$$

where α_i and α_i^* denote the Lagrangian multipliers, and $K(\mathbf{x}_i, \mathbf{x}) = \phi(\mathbf{x}_i)\phi(\mathbf{x})$ is the kernel function [69,70,73]. In this study, Radial Basis Function (RBF) kernel is used for the SVR method (Eq. (11)).

$$K(\mathbf{x}, \mathbf{x}_i) = \exp\left(-\frac{\| \mathbf{x} - \mathbf{x}_i \|}{2\sigma^2}\right) \tag{11}$$

3. Results and discussions

3.1. Correlation assessments

Assessing relationships for ranking variables based on their effectiveness could provide insights into the model and explain it. Pearson correlation and SHAP analyses were used throughout the entire dataset for the relationship assessments. In a plant, when the process is working on its steady-state, there are several interactions between variables; SHAP would be about to consider

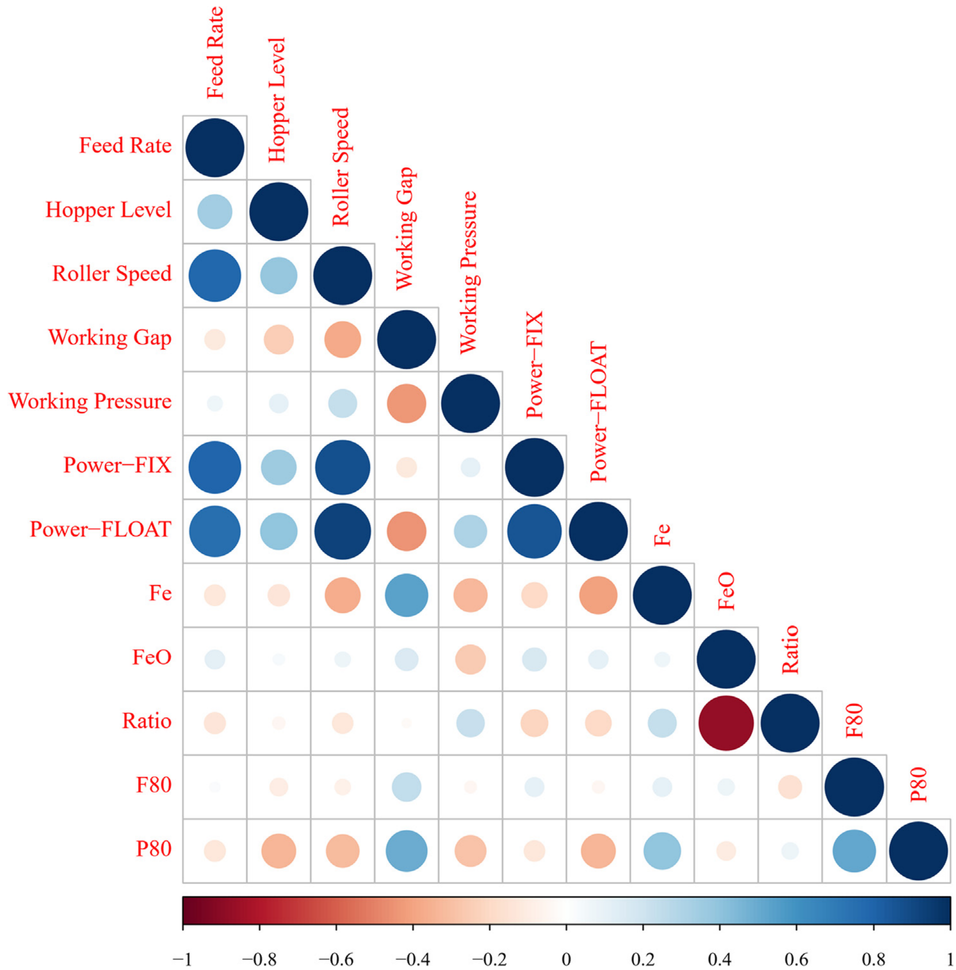

Fig. 3. Pearson correlation between HPGR parameters.

all these interactions based on the existing monitored variables that come from units. SHAP analyses (Fig. 2) demonstrated that in the steady-state conditions of operating the HPGR, the working gap within all the variables in the dataset had the highest importance for the P_{80} prediction. In contrast, the working pressure had the lowest rank of importance. SHAP values showed the magnitude relationship between P_{80} and the working gap is positive. In other words, a lower working gap would result in a smaller particle size. It is well understood that a larger working gap would contain larger particles unbroken pass through the rolls [19]; however, the HPGR operator cannot directly control the gap to achieve the desired P_{80}. The larger working gap would permit larger particles to pass through unbroken. F_{80} received the second rank of importance for the prediction and positively correlated with P_{80} (Fig. 2).

A strong consistency could be observed between SHAP and Pearson correlation results (Figs. 2–3). Working gap and F_{80} showed the highest inter-correlation (positive relationships) with P_{80} (their lower values could lead to a finer particle size production). Pearson correlation also indicated a positive linear relationship between the working gap and F_{80}. Coarser feed particles led to larger products. The coarsest feed particles that could be accepted within the rolls would also affect the working gap and might localize rolls by stressing them and pushing the hydro-pneumatic spring [74]. In other words, coarser feed top sizes could lead to a larger working gap [19]. SHAP analyses (Fig. 4) illustrated a nonlinear positive relationship between them (based on all the recorded data points). In general, SHAP could assess multivariable relationships, plotted SHAP values for each point of variables, considered for their ranking. In contrast, Pearson correlation only could evaluate a single linear relationship between two features and plot the effect of variables (not each record) on the output.

In HPGRs, the feed properties (particle properties: size, composition, hardness, etc.) could interact with the hydro-pneumatic spring and determine the working gap. As SHAP and Pearson correlation results indicated (Figs. 2–4), there are several different multi interactions among the HPGR operating variables. Results (Fig. 3) showed that there is a negative correlation between roller speed and working gap. Lim et al. (1997) showed when the roll speed increased, the working gap decreased. They reported that this correlation is stronger than the relationship between the working gap and the specific grinding force [19]. Lubjuhn and Schoenert (1993) noted that the negative relationship between roller speed and the working gap increases the particles' enhancing slip in the acceleration zone [75]. Figs. 2–4 illustrated their negative relationships. $\frac{Fe}{FeO}$ ratio showed a positive correlation with the P_{80} production (Fig. 2). In other words, increasing the Fe and decreasing the FeO could lead to a coarser production (a higher P_{80}) (Figs. 2–4). Although this ratio is an intrinsic property of the feed material, results showed that it affects the P80 and could be used for its prediction. Increasing this ratio represented higher hematite than magnetite in the feed, which could cause a higher ore toughness, lower grindability, and potentially a higher P_{80}. Hopper level indicated a negative relationship with the P_{80} (Figs. 2–3). Rule et al. (2008) reported that achieving a preferred HPGR hopper level would be difficult if the

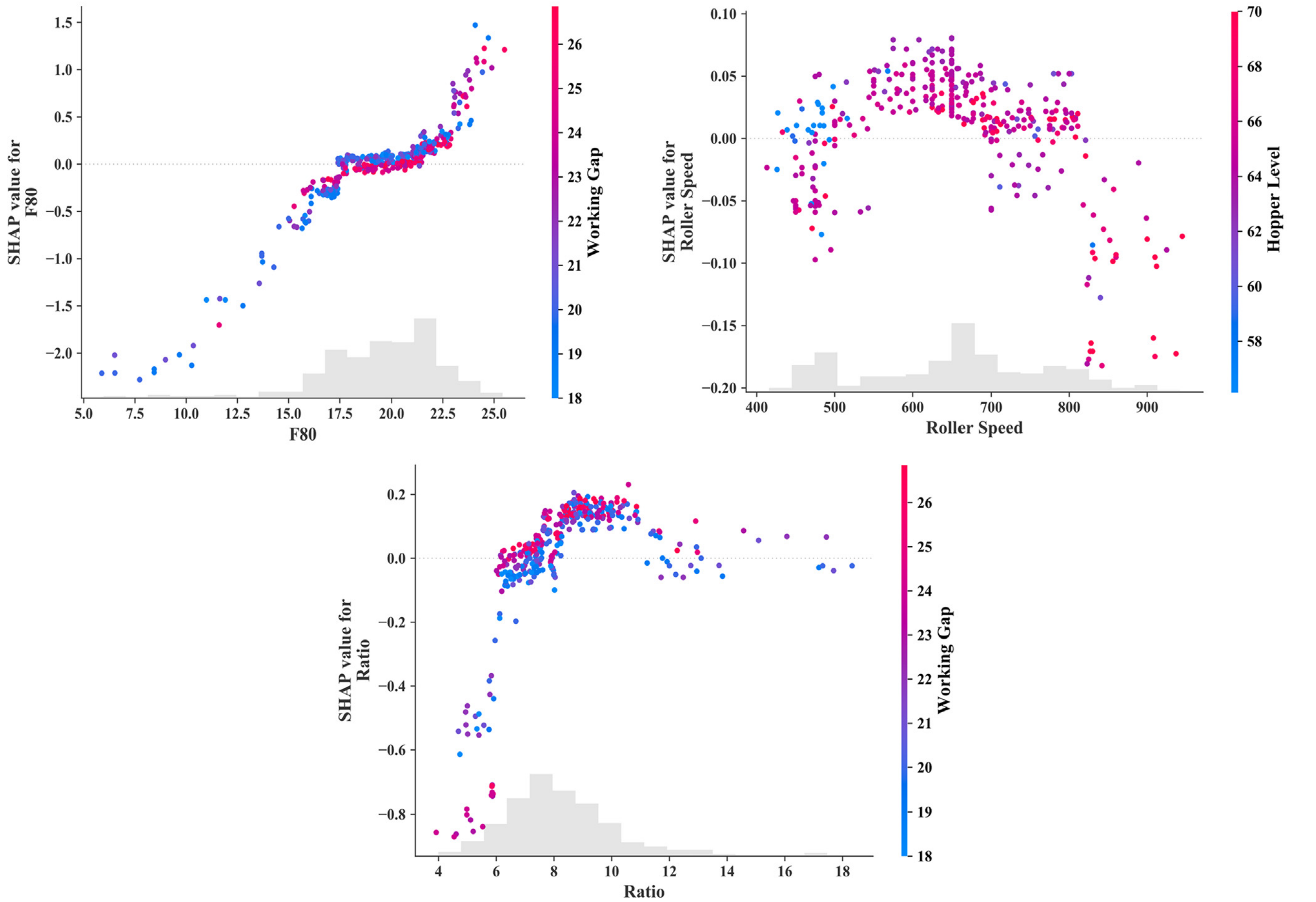

Fig. 4. SHAP correlation assessments between F_{80} and working gap (blue dots: lower value and red dots: higher values). (For interpretation of the references to colour in this figure legend, the reader is referred to the web version of this article.)

HPGR unit was not fitted with variable speed driven [76]. Thus, this negative relationship could be due to a positive inter-correlation between the hopper level and roller speed (Figs. 2–4). It was documented that increasing the roller speed (in a limited range) could lead to overall finer iron ore products [19]. Power draw (Fixed and Float) and roller speed showed negative correlations with the P_{80} (their increases generated finer particles). Moreover, results showed that the power draw increased by increasing the roller speed (Figs. 2–3). This positive correlation was reported in the other investigations [26,77]. Feed rate and working pressure indicated insignificant relationships with the P_{80}; however, it was noted that they have to be used for modeling HPGR products to cover all possible multi interactions [26,78].

3.2. P_{80} prediction

From the entire dataset, around 80% of records were randomly considered for the training stage of the XGBoost models to predict the P_{80}. The rest of the remained data was considered for the model's testing stage. Several different optimum model features were examined, and they were adjusted and applied for training after the tuning process. The four main XGBoost hyperparameters are general, booster, learning task, and command-line parameters. General parameters are the overall functioning of the XGBoost model and include booster, verbosity, and nthread. From booster parameters, gbtree, gblinear, or dart can be selected. The verbosity of printing messages could be 0 (silent), 1 (warning), 2 (info), 3 (debug). The nthread can be used for parallel processing. The number of cores in the system has to be entered. The value should not be

Table 2
The XGBoost parameter settings for the P_{80} prediction.

Parameter	Value (Type)
Base learner	Gradient boosted tree
Tree construction algorithm	Exact greedy
Learning objective	Regression with squared loss
Learning rate (η)	0.108
Lagrange multiplier (γ)	6.1
Number of boosted trees	45
Maximum depth of trees	7
Minimum sum of weights required for a node to split into a child	1
Maximum delta step allowed each leaf output to be	0 (There is no constraint)

Table 3
Provided accuracy by the different examined machine learning methods in the testing phase.

Method		R-square	RMSE*
Random Forest	Number of Trees = 20	0.76	0.80
Support Vector Regression	Kernel = RBF	0.69	0.89
XGBoost		**0.83**	**0.67**

* Root mean square error.

entered for running on all cores, and the algorithm would detect automatically. Tree and linear boosters are the XGBoost booster parameters. Tree booster typically outperforms the linear booster. Learning task parameters corresponded to the learning objective and define the optimization objective that needs to be calculated for the metric at each step. In this work, the hyperparameters were considered mainly the default of its algorithm. After the tuning process (a try and error procedure), the optimum model features are adjusted and applied for training (Table 2).

The XGBoost results in the testing step (Table 3) indicated that XGBoost could quite accurately estimate the HPGR P_{80} stand on the monitored operational parameters. RF and SVR models were considered to the P80 prediction with the same training and testing sets for comparison purposes Outcomes (Table 3) demonstrated that the XGBoost model provided suggestively higher accuracy than these two known ML models for the P_{80} prediction (Fig. 5). These results indicated that SHAP- XGBoost could successfully construct a CL for an HPGR unit as a commanding EAI system. These comprehensive results potentially depicted that this model could be used for modeling, controlling, and maintaining different HPGR circuits on an industrial scale.

4. Conclusions

Developing a conscious lab for size reduction units in mineral processing plants and move toward digitalizing operational systems would increase the process efficiency and improve process control and maintenance. Using explainable artificial intelligence models as novel algorithms for constructing a conscious lab could translate big industrial datasets to a piece of understandable human basis information. Outcomes of this investigation indicated that SHAP and XGBoost (as most recent explainable artificial intelligence tools for developing a conscious lab) could accurately model relationships between operational variables of an industrial High-Pressure Grinding Roll. SHAP analyses noted that within the steady-state operational conditions, the working gap showed the highest nonlinear correlation (positive) with the particle size production (P_{80}) and ranked as the most effective factor for the P_{80}. SHAP could accurately address all multi interactions and relationship magnitudes between operational and feed properties. XGBoost united with SHAP could accurately predict the P_{80} based on the monitoring parameters in the plant (root mean square error < 0.7). Comparing SHAP-XGBoost results with typical modeling (Pearson correlation, random forest, and support vector regression) demonstrated that coupling these two powerful methods could successfully be used for developing conscious labs for different advanced powder technologies.

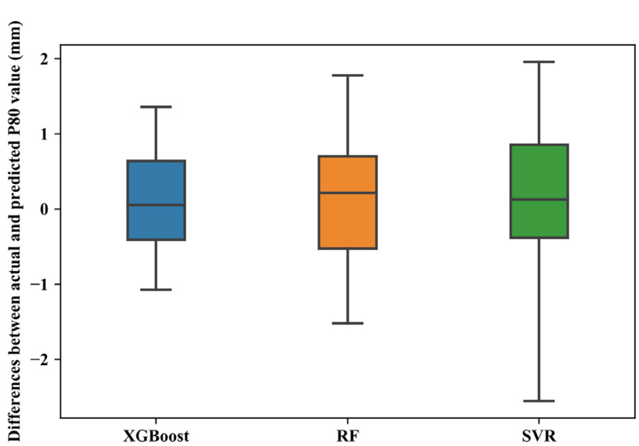

Fig. 5. Differences between actual and predicted P_{80} by AI methods in the testing phase.

CRediT authorship contribution statement

S. Chehreh Chelgani: Conceptualization, Methodology, Software, Validation, Formal analysis, Investigation, Writing – original draft, Writing – review & editing. **H. Nasiri:** Conceptualization, Methodology, Software, Validation, Formal analysis, Investigation, Writing – original draft, Writing – review & editing. **A. Tohry:** Conceptualization, Methodology, Validation, Formal analysis, Resources.

Declaration of Competing Interest

The authors declare that they have no known competing financial interests or personal relationships that could have appeared to influence the work reported in this paper.

References

[1] D.W. Fuerstenau, A.-Z.-M. Abouzeid, Role of feed moisture in high-pressure roll mill comminution, Int. J. Miner. Process. 82 (4) (2007) 203–210.
[2] K. Schönert, A first survey of grinding with high-compression roller mills, Int. J. Miner. Process. 22 (1-4) (1988) 401–412.
[3] D. Saramak, T. Tumidajski, M. Brożek, T. Gawenda, Z. Naziemiec, Aspects of comminution flowsheets design in processing of mineral raw materials, Gospod. Surowcami Miner. 26 (2010) 59–69.
[4] M.J. Daniel, S. Morrell, HPGR model verification and scale-up, Miner. Eng. 17 (11-12) (2004) 1149–1161.
[5] A.-Z. Abouzeid, D.W. Fuerstenau, Grinding of mineral mixtures in high-pressure grinding rolls, Int. J. Miner. Process. 93 (1) (2009) 59–65.
[6] V. Hasanzadeh, A. Farzanegan, Robust HPGR model calibration using genetic algorithms, Miner. Eng. 24 (5) (2011) 424–432.
[7] H. Dundar, H. Benzer, N. Aydogan, Application of population balance model to HPGR crushing, Miner. Eng. 50-51 (2013) 114–120.
[8] D. Saramak, R.A. Kleiv, The effect of feed moisture on the comminution efficiency of HPGR circuits, Miner. Eng. 43-44 (2013) 105–111.
[9] J.A. Drozdiak, A pilot-scale examination of a novel high pressure grinding roll/stirred mill comminution circuit for hard-rock mining applications, University of British Columbia, 2011.
[10] G. Li, R. Roufail, B. Klein, L. Nordell, A. Kumar, C. Sun, J. Kou, Experimental evaluation of the conjugate anvil hammer mill–Comparison of semi-confined to confined particle breakage, Miner. Eng. 137 (2019) 34–42.
[11] M. Johansson, M. Evertsson, A time dynamic model of a high pressure grinding rolls crusher, Miner. Eng. 132 (2019) 27–38.
[12] Y.-W. Li, L.-L. Zhao, E.-Y. Hu, K.-K. Yang, J.-F. He, H.-S. Jiang, Q.-F. Hou, Laboratory-scale validation of a DEM model of a toothed double-roll crusher and numerical studies, Powder Technol. 356 (2019) 60–72.
[13] G.K.P. Barrios, L.M. Tavares, A preliminary model of high pressure roll grinding using the discrete element method and multi-body dynamics coupling, Int. J. Miner. Process. 156 (2016) 32–42.
[14] P.W. Cleary, M.D. Sinnott, Axial pressure distribution, flow behaviour and breakage within a HPGR investigation using DEM, Miner. Eng. 163 (2021) 106769.
[15] Y. Nagata, Y. Tsunazawa, K. Tsukada, Y. Yaguchi, Y. Ebisu, K. Mitsuhashi, C. Tokoro, Effect of the roll stud diameter on the capacity of a high-pressure grinding roll using the discrete element method, Miner. Eng. 154 (2020) 106412.
[16] D.W. Fuerstenau, A. Shukla, P.C. Kapur, Energy consumption and product size distributions in choke-fed, high-compression roll mills, Int. J. Miner. Process. 32 (1-2) (1991) 59–79.
[17] L.G. Austin, K.R. Weller, W.I.L. Lim, Phenomenological modelling of the high pressure grinding rolls, in: XVIII Int. Miner. Process. Congr., AUSIMM, Sydney, 1993: pp. 87–96.
[18] L.G. Austin, M.P. Trubeljal, H.M. Von Seebach, Capacity of high-pressure grinding rolls, Mining, Metall. & Explor. 12 (1995) 65–73.
[19] W.I.L. Lim, J.J. Campbell, L.A. Tondo, The effect of rolls speed and rolls surface pattern on high pressure grinding rolls performance, Miner. Eng. 10 (4) (1997) 401–419.
[20] W.I.L. Lim, K.R. Weller, Some benefits of using studded surfaces in high pressure grinding rolls, Miner. Eng. 12 (2) (1999) 187–203.
[21] S. Morrell, W. Lim, F. Shi, L. Tondo, Modelling of the HPGR Crusher, Comminution Pract. (1997) 117–126.
[22] M. Torres, A. Casali, A novel approach for the modelling of high-pressure grinding rolls, Miner. Eng. 22 (13) (2009) 1137–1146.
[23] C.L. Schneider, V.K. Alves, L.G. Austin, Modeling the contribution of specific grinding pressure for the calculation of HPGR product size distribution, Miner. Eng. 22 (7-8) (2009) 642–649.
[24] T.M. Campos, G. Bueno, L.M. Tavares, Modeling comminution of iron ore concentrates in industrial-scale HPGR, Powder Technol. 383 (2021) 244–255.
[25] G. Pamparana, B. Klein, A methodology to predict the HPGR operational gap by using piston press tests, Miner. Eng. 166 (2021) 106875.

[26] A. Tohry, S. Yazdani, E. Hadavandi, E. Mahmudzadeh, S.C. Chelgani, Advanced modeling of HPGR power consumption based on operational parameters by BNN: A "Conscious-Lab" development, Powder Technol. 381 (2021) 280–284.
[27] M. Alidokht, S. Yazdani, E. Hadavandi, S.C. Chelgani, Modeling metallurgical responses of coal Tri-Flo separators by a novel BNN: a "Conscious-Lab" development, Int. J. Coal Sci. & Technol. (2021) 1–11.
[28] G. Vilone, L. Longo, Notions of explainability and evaluation approaches for explainable artificial intelligence, Inf. Fusion. 76 (2021) 89–106, https://doi.org/10.1016/j.inffus.2021.05.009.
[29] R. Dazeley, P. Vamplew, C. Foale, C. Young, S. Aryal, F. Cruz, Levels of Explainable Artificial Intelligence for Human-Aligned Conversational Explanations, Artif. Intell. 299 (2021) 103525, https://doi.org/10.1016/j.artint.2021.103525.
[30] S.M. Lundberg, S.-I. Lee, A unified approach to interpreting model predictions, in: Proc. 31st Int. Conf. Neural Inf. Process. Syst., 2017, pp. 4768–4777.
[31] S.C. Chelgani, Estimation of gross calorific value based on coal analysis using an explainable artificial intelligence, Mach. Learn. with Appl. 6 (2021) 100116, https://doi.org/10.1016/j.mlwa.2021.100116.
[32] S. Mangalathu, S.-H. Hwang, J.-S. Jeon, Failure mode and effects analysis of RC members based on machine-learning-based SHapley Additive exPlanations (SHAP) approach, Eng. Struct. 219 (2020) 110927.
[33] H. Mao, X. Deng, H. Jiang, L. Shi, H. Li, L. Tuo, D. Shi, F. Guo, Driving safety assessment for ride-hailing drivers, Accid. Anal. & Prev. 149 (2021) 105574.
[34] H. Park, D.Y. Park, Comparative analysis on predictability of natural ventilation rate based on machine learning algorithms, Build. Environ. 195 (2021) 107744.
[35] K. Zhou, S. Li, X. Zhou, Y. Hu, C. Zhang, J. Liu, Data-driven prediction and analysis method for nanoparticle transport behavior in porous media, Measurement 172 (2021) 108869.
[36] J. Zhou, Y. Qiu, S. Zhu, D.J. Armaghani, M. Khandelwal, E.T. Mohamad, Estimation of the TBM advance rate under hard rock conditions using XGBoost and Bayesian optimization, Undergr. Sp. (2020).
[37] Z. Zhang, Y. Huang, R. Qin, W. Ren, G. Wen, XGBoost-based on-line prediction of seam tensile strength for Al-Li alloy in laser welding: Experiment study and modelling, J. Manuf. Process. 64 (2021) 30–44.
[38] R. Zhong, R. Johnson Jr, Z. Chen, Generating pseudo density log from drilling and logging-while-drilling data using extreme gradient boosting (XGBoost), Int. J. Coal Geol. 220 (2020) 103416.
[39] Z. Feng, N. Guan, M. Lv, W. Liu, Q. Deng, X. Liu, W. Yi, Efficient drone hijacking detection using two-step GA-XGBoost, J. Syst. Archit. 103 (2020) 101694.
[40] H. Dong, D. He, F. Wang, SMOTE-XGBoost using Tree Parzen Estimator optimization for copper flotation method classification, Powder Technol. 375 (2020) 174–181.
[41] S. Mangalathu, H. Shin, E. Choi, J.-S. Jeon, Explainable machine learning models for punching shear strength estimation of flat slabs without transverse reinforcement, J. Build. Eng. 39 (2021) 102300.
[42] A. Movsessian, D.G. Cava, D. Tcherniak, Interpretable machine learning in damage detection using Shapley Additive Explanations, 2021.
[43] N. Bussmann, P. Giudici, D. Marinelli, J. Papenbrock, Explainable machine learning in credit risk management, Comput. Econ. 57 (1) (2021) 203–216.
[44] T. Chen, C. Guestrin, Xgboost: A scalable tree boosting system, in: Proc. 22nd ACM SIGKDD Int. Conf. Knowl. Discov. Data Min., 2016, pp. 785–794.
[45] Y. Xu, X. Zhao, Y. Chen, Z. Yang, Research on a Mixed Gas Classification Algorithm Based on Extreme Random Tree, Appl. Sci. 9 (2019) 1728.
[46] A. Ogunleye, Q.-G. Wang, XGBoost model for chronic kidney disease diagnosis, IEEE/ACM Trans. Comput. Biol. Bioinforma. 17 (6) (2020) 2131–2140.
[47] K. Song, F. Yan, T. Ding, L. Gao, S. Lu, A steel property optimization model based on the XGBoost algorithm and improved PSO, Comput. Mater. Sci. 174 (2020) 109472.
[48] H. Nasiri, S. Hasani, Automated detection of COVID-19 cases from chest X-ray images using deep neural network and XGBoost, ArXiv Prepr, ArXiv:2109.02428. 2021. http://arxiv.org/abs/2109.02428.
[49] R.P. Sheridan, W.M. Wang, A. Liaw, J. Ma, E.M. Gifford, Extreme gradient boosting as a method for quantitative structure–activity relationships, J. Chem. Inf. Model. 56 (12) (2016) 2353–2360.
[50] H. Wang, C. Liu, L. Deng, Enhanced prediction of hot spots at protein-protein interfaces using extreme gradient boosting, Sci. Rep. 8 (2018) 1–13.
[51] W. Zhang, C. Wu, H. Zhong, Y. Li, L. Wang, Prediction of undrained shear strength using extreme gradient boosting and random forest based on Bayesian optimization, Geosci. Front. 12 (1) (2021) 469–477.
[52] J. Ma, Y. Ding, J.C.P. Cheng, Y. Tan, V.J.L. Gan, J. Zhang, Analyzing the leading causes of traffic fatalities using XGBoost and grid-based analysis: a city management perspective, IEEE Access 7 (2019) 148059–148072.
[53] S.S. Matin, J.C. Hower, L. Farahzadi, S.C. Chelgani, Explaining relationships among various coal analyses with coal grindability index by Random Forest, Int. J. Miner. Process. 155 (2016) 140–146.
[54] S.C. Chelgani, S.S. Matin, Study the relationship between coal properties with Gieseler plasticity parameters by random forest, Int. J. Oil, Gas Coal Technol. 17 (1) (2018) 113, https://doi.org/10.1504/IJOGCT.2018.089345.
[55] L. Breiman, Random forests, Mach. Learn. 45 (2001) 5–32.
[56] L. Breiman, Bagging predictors, Mach. Learn. 24 (1996) 123–140.
[57] Y. Amit, D. Geman, Shape quantization and recognition with randomized trees, Neural Comput. 9 (7) (1997) 1545–1588.
[58] A. Tohry, S. Chehreh Chelgani, S.S. Matin, M. Noormohammadi, Power-draw prediction by random forest based on operating parameters for an industrial ball mill, Adv. Powder Technol. 31 (3) (2020) 967–972.
[59] S.S. Matin, S.C. Chelgani, Estimation of coal gross calorific value based on various analyses by random forest method, Fuel 177 (2016) 274–278.
[60] B. Shahbazi, S. Chehreh Chelgani, S.S. Matin, Prediction of froth flotation responses based on various conditioning parameters by Random Forest method, Colloids Surfaces A Physicochem. Eng. Asp. 529 (2017) 936–941.
[61] S. Nazari, S. Chehreh Chelgani, S.Z. Shafaei, B. Shahbazi, S.S. Matin, M. Gharabaghi, Flotation of coarse particles by hydrodynamic cavitation generated in the presence of conventional reagents, Sep. Purif. Technol. 220 (2019) 61–68.
[62] E. Scornet, G. Biau, J.-P. Vert, others, Consistency of random forests, Ann. Stat. 43 (2015) 1716–1741.
[63] S. Wager, S. Athey, Estimation and inference of heterogeneous treatment effects using random forests, J. Am. Stat. Assoc. 113 (523) (2018) 1228–1242.
[64] J. Zhou, E. Li, H. Wei, C. Li, Q. Qiao, D.J. Armaghani, Random forests and cubist algorithms for predicting shear strengths of rockfill materials, Appl. Sci. 9 (2019) 1621.
[65] P. Bühlmann, B. Yu, et al., Analyzing bagging, Ann. Stat. 30 (2002) 927–961.
[66] H. Drucker, C.J.C. Burges, L. Kaufman, A. Smola, V. Vapnik, others, Support vector regression machines, Adv. Neural Inf. Process. Syst. 9 (1997) 155–161.
[67] E. Hadavandi, S.C. Chelgani, Estimation of coking indexes based on parental coal properties by variable importance measurement and boosted-support vector regression method, Measurement 135 (2019) 306–311.
[68] M. Awad, R. Khanna, Support vector regression, in: Effic. Learn. Mach., Springer, 2015, pp. 67–80.
[69] E. Hadavandi, J.C. Hower, S.C. Chelgani, Modeling of gross calorific value based on coal properties by support vector regression method, Model. Earth Syst. Environ. 3 (2017) 1–7.
[70] J. Wei, G. Dong, Z. Chen, Remaining useful life prediction and state of health diagnosis for lithium-ion batteries using particle filter and support vector regression, IEEE Trans. Ind. Electron. 65 (7) (2018) 5634–5643.
[71] D.i. Zhang, J. Lin, Q. Peng, D. Wang, T. Yang, S. Sorooshian, X. Liu, J. Zhuang, Modeling and simulating of reservoir operation using the artificial neural network, support vector regression, deep learning algorithm, J. Hydrol. 565 (2018) 720–736.
[72] Z. Zhang, W.-C. Hong, Electric load forecasting by complete ensemble empirical mode decomposition adaptive noise and support vector regression with quantum-based dragonfly algorithm, Nonlinear Dyn. 98 (2) (2019) 1107–1136.
[73] S. Chehreh Chelgani, B. Shahbazi, E. Hadavandi, Support vector regression modeling of coal flotation based on variable importance measurements by mutual information method, Measurement 114 (2018) 102–108.
[74] K. Schönert, The characteristics of comminution with high pressure roller mills, KONA Powder Part. J. 9 (0) (1991) 149–158.
[75] U. Lubjuhn, K. Schönert, Material flow in the acceleration zone and throughput of high pressure roller mills, in: XVIII Int. Miner. Process. Congr. (IMPC), Sydney, 1993, pp. 161–168.
[76] C.M. Rule, D.M. Minnaar, G.M. Sauermann, HPGR-revolution in platinum?, J South. African Inst. Min. Metall. 109 (2009) 23–30.
[77] F. der Meer, High pressure grinding rolls scale-up and experiences, in: XXV Int. Miner. Process. Congr. (IMPC), Brisbane, 2010, pp. 1319–1331.
[78] S. Morrell, Predicting the overall specific energy requirement of crushing, high pressure grinding roll and tumbling mill circuits, Miner. Eng. 22 (6) (2009) 544–549.